Memoirs of the Faculty of Engineering, Kyushu University, Vol. 35, No. 3, Feb. 1976

# Analyses of Boundary-Value Problems by Means of Green's Identity Formula for Two-Dimensional Waves of Finite Water Depth

——Permeable and Impermeable Coastal Structures with Arbitrary Cross-Sections——

by

Takeshi IJIMA* and Chung Ren CHOU**

(Received October 13, 1975)

**Abstract**

A method of numerical analysis which is simplified by means of Green's identity formula is proposed for the analyses of two-dimensional boundary-value problems of small amplitude waves in finite water depth.

$\log(1/r)$ is a particular solution of Laplace's equation in two-dimensional bounded domain, if $r$ is the distance between an interior point and the point on the closed boundary. Hence, using $\log(1/r)$ as one potential function, another arbitrary potential function at a point in that domain is expressed by its values and normal derivatives on the boundary, by means of Green's theorem. And, taking the limit when the interior point approaches to the boundary point, an integral equation with respect to the boundary-values and normal derivatives of that function is provided. So that, if another relationship between them is defined mechanically, above quantities on the boundary are to be determined. Since the mechanical boundary conditions are always linear in small amplitude wave problems, two-dimensional boundary-value problems are easily analyzed numerically by this principle.

As examples of application, this paper presents the formulation and numerical results for wave transformation by permeable breakwater, seawall and submerged breakwater of arbitrary cross-sections, by linearizing the fluid resistance in porous material so as to be proportional to the fluid velocities.

The problems for those structures with vertical faces were solved by another method of continuation of velocity potentials by one of the authors, and they are, of course, analyzed as a special case of this proposed method. It is certified that the results of these two methods are in perfect agreement, so that the wave transformation at above structures with arbitrary sloped-faces can be estimated by the proposed method, with appropriate values of coefficient of fluid resistance in porous material.

Moreover, it is shown that wave transformation by gradual change of water depth and beach profile, and wave action to the submerged impermeable body of arbitrary cross-section is easily analyzed as a simple case of this method.

## I Introduction

The authors (1971) have been investigated the problem of wave transformation by permeable breakwater and seawall with vertical faces, by the method of continuation of velocity potentials. Similar method of investigation to the authors' method was published by Sollitt (1972) and the author's

* Professor of Hydraulic Civil Engineering
** Master of Engineering, Graduate Student of Hydraulic Civil Engineering

results are proved to be reasonable.

However, above investigations are limitted to the case for vertical-face structures which are rarely used in actual field. Hence, it is desired to analyze the problem on usual sloped-face breakwater and seawall. Sollitt (1972) proposed a rough estimation on above problems, and Mccoquodale (1972) has investigated numerically by means of finite element method. However, the former investigation seems to be too conventional to discuss the effect of sloped-faces and the latter is too complicated and takes much time in calculation even for one type of structures and an incident wave characteristics, so that it seems to be unsuitable for their investigations to obtain general considerations on wave transformation by various types of structures and various incident waves.

This paper proposes a numerical method of analysis which is extremely simplified by means of Green's identity formula for two-dimensional wave problems and presents the formulation and numerical results mainly on the permeable structures of sloped-faces, as application examples of our method.

According to the Green's thoerem, the value of a potential function at a point in two-dimensional bounded domain is expressed by its boundary values and its normal derivatives to the boundary, if $\log(1/r)$ is used as a particular solution of Laplace's equation, taking $r$ as the distance of the interior point and that on the closed boundary. And, to the extreme case when the interior point approaches to a boundary point, it follows that a linear integral equation is given with respect to the potentials and its normal derivatives on the boundary. This equation is dependent solely on the shape of the domain, so that it defines geometrically the relation between potential value and its normal derivative on the boundary. Hence, if another system of linear relations between them is defined by mechanical boundary conditions, it is possible to determine them by solving above geometrical and mechanical relations, simultaneously. As long as the mechanical boundary condition is linear with respect to potential values and normal derivatives, above principle of analysis is generally applied to the boundary-value problems.

## II Green's identity formula

Assuming that a function $\phi(x, z)$ satisfies the Laplace's equation in the domain enclosed by a closed curve $D$ and that it has continuous second order derivatives, it follows that the potential function at an interior point $(x, z)$ is expressed by its values on the boundary curve $\phi(\xi, \eta)$ and its outward normal derivatives to the boundary $\partial\phi(\xi, \eta)/\partial\nu$ as follows:

$$\phi(x, z) = \frac{1}{2\pi}\int_D \left[\phi(\xi, \eta)\frac{\partial}{\partial(\nu/h_0)}\log(r/h_0) - \frac{\partial\phi(\xi, \eta)}{\partial(\nu/h_0)}\cdot\log(r/h_0)\right] ds/h_0 \tag{2.1}$$

where $r$ is the distance between the interior point $(x, z)$ and the bounary point $(\xi, \eta)$, $h_0$ is a constant reference length to the size of the closed domain (e.g. the water depth), $\nu$ is outward normal to the boundary and integral denotes the line integral in counter-clockwise direction along the boundary $D$.

To the extreme case when the point $(x, z)$ approaches to the point $(\xi', \eta')$ on the boundary, the following integral equation is derived from Eq. (2.1):

$$\phi(\xi', \eta') = \frac{1}{\pi}\int_D \left[\phi(\xi, \eta)\cdot\frac{\partial}{\partial(\nu/h_0)}\log(R/h_0) - \frac{\partial\phi(\xi, \eta)}{\partial(\nu/h_0)}\cdot\log(R/h_0)\right] ds/h_0 \tag{2.2}$$

where $R$ indicates the distance between the point $(\xi, \eta)$ and $(\xi', \eta')$.

If we divide the boundary curve $D$ into $N$ small segments by $N$ points and indicate the central point and the length of each segment by $(\xi_j, \eta_j)$ $(j=1\sim N)$ and by $\Delta S_j$, it follows that Eq. (2.2) is reduced to the following difference equation:

$$\phi(i) = \sum_{j=1}^{N}\left[\bar{E}_{ij}\phi(j) - E_{ij}\bar{\phi}(j)\right] \qquad (i=1\sim N) \tag{2.3}$$

where $\phi(j)$, $\bar{\phi}(j)$ denote the values at point $(\xi_j, \eta_j)$ and $\bar{\phi}(j)=\partial\phi(j)/\partial(\nu/h_0)$. $E_{ij}$ and $\bar{E}_{ij}$ are the integrated values as defined by the following expressions:

$$E_{ij}=\frac{1}{\pi}\int_{\Delta S_j}\log(R_{ij}/h_0)\cdot ds/h_0,\quad \bar{E}_{ij}=\frac{1}{\pi}\int_{\Delta S_j}\frac{\partial}{\partial(\nu/h_0)}\log(R_{ij}/h_0)\cdot ds/h_0$$
$$R_{ij}=\sqrt{(\xi_j-\xi_i)^2+(\eta_j-\eta_i)^2} \tag{2.4}$$

Eq. (2.3) yields a system of linear equations with respect to $\phi$ and $\bar{\phi}$ on the boundary. They are dependent solely on the shape of the domain, so that provide the geometrical relations between $\phi$ and $\bar{\phi}$.

The value of the potential function at interior point $(x, z)$ is calculated by means of Eq. (2.1) as follows:

$$\phi(x, z)=\frac{1}{2}\sum_{j=1}^{N}(\bar{E}_{X,j}\phi(j)-E_{X,j}\bar{\phi}(j)) \tag{2.5}$$

where

$$E_{Xj}=\frac{1}{\pi}\int_{\Delta S_j}\log(r_{Xj}/h_0)ds/h_0,\quad \bar{E}_{Xj}=\frac{1}{\pi}\int_{\Delta S_j}\frac{\partial}{\partial(\nu/h_0)}\log(r_{Xj}/h_0)\,ds/h_0$$
$$r_{Xj}=\sqrt{(\xi_j-x)^2+(\eta_j-z)^2} \tag{2.6}$$

## III Dynamical and kinematical boundary conditions for small amplitude waves in finite water depth

Now, we consider small amplitude wave motions in incompressible, inviscid fluid and those in porous materials.

We take the origin of coordinate system O at still water surface, $x$-axis in horizont, $z$-axis vertically upwards, and indicate the time and gravity acceleration by $t$ and $g$, respectively. The amplitude and frequency of incident wave are denoted by $\zeta_0$ and $\sigma$ ($=2\pi/T$: $T$ is wave period), respectively.

(i) Wave motion in incompressible, inviscid fluid

Putting the velocity potential of fluid motion as $\Phi(x, z; t)=\frac{g\zeta_0}{\sigma}\phi(x, z)e^{i\sigma t}$, it follows that the potential function $\phi(x, z)$ satisfies the following Laplace's equation:

$$\partial^2\phi/\partial x^2+\partial^2\phi/\partial z^2=0 \tag{3.1}$$

Horizontal and vertical fluid velocities $u$, $w$, fluid pressure $p$ and surface wave profile $\zeta$ are provided, indicating the fluid density by $\rho$, as follows:

$$u=\frac{\partial\Phi}{\partial x},\quad w=\frac{\partial\Phi}{\partial z},\quad \frac{p}{\rho g\zeta_0}=-i\phi(x, z)e^{i\sigma t},\quad \frac{\zeta}{\zeta_0}=-i\phi(x, 0)e^{i\sigma t} \tag{3.2}$$

Boundary conditions in our problems are as follows:

(a) Free surface boundary condition

Combining the dynamical condition of constant pressure and kinematical condition, the free surface boundary condition is yielded by the following equation:

$$\frac{\partial\phi}{\partial z}=\frac{\sigma^2}{g}\phi \quad \text{and so} \quad \bar{\phi}=\frac{\partial\phi}{\partial(\nu/h_0)}=\frac{\sigma^2h_0}{g}\phi \quad \text{at} \quad z=0 \tag{3.3}$$

(b) Boundary condition at rigid surface

Fluid velocity normal to rigid surface should be vanished, so that

$$\frac{\partial \phi}{\partial \nu}=0 \quad \text{and so} \quad \bar{\phi}=\frac{\partial \phi}{\partial(\nu/h_0)}=0 \quad \text{at rigid surface} \tag{3.4}$$

(ii) Wave motion in porous materials

It is considered that the fluid motion in porous materials like permeable breakwater and seawall is imposed by a resistance proportional to the square of the fluid velocity and by the one proportional to the local fluid acceleration. Linearizing the former so as to be proportional to the fluid velocity with proportional constant $\mu$, making the latter to be included in the virtual porosity $V$ and indicating the horizontal and vertical macroscopic fluid velocities by $u_*$, $w_*$, fluid pressure by $p_*$, it follows that the equation of continuity and horizontal and vertical equations of motion are yielded as follows:

$$\frac{\partial u_*}{\partial x}+\frac{\partial w_*}{\partial z}=0 \tag{3.5}$$

$$\frac{1}{V}\frac{\partial u_*}{\partial t}=-\frac{1}{\rho}\frac{\partial p_*}{\partial x}-\frac{\mu}{V}u_* \tag{3.6}$$

$$\frac{1}{V}\frac{\partial w_*}{\partial t}=-\frac{1}{\rho}\frac{\partial p_*}{\partial z}-\frac{\mu}{V}w_*-g \tag{3.7}$$

Above fluid motion has a velocity potential $\Phi_*(x, z; t)=\frac{g\zeta_0}{\sigma}\phi_*(x, z)e^{i\sigma t}$, by which fluid velocities, pressure and free surface wave profile are provided as follows:

$$\begin{gathered} u_*=\frac{\partial \Phi_*}{\partial x}, \quad w_*=\frac{\partial \Phi_*}{\partial z}, \quad \frac{p_*}{\rho g\zeta_0}=-i\beta\phi_*(x, z)e^{i\sigma t} \\ \frac{\zeta_*}{\zeta_0}=-i\beta\phi_*(x, 0)e^{i\sigma t} \quad \text{where} \quad \beta=\frac{\alpha}{V}, \quad \alpha=1-i\mu/\sigma \end{gathered} \tag{3.8}$$

Boundary conditions are obtained as follows:

(a) Free surface boundary condition

Combining the kinematical condition on free surface $\frac{\partial \zeta_*}{\partial t}=\frac{1}{V}\frac{\partial \Phi_*}{\partial z}$ at $z=0$ with the constant pressure condition, the following relation is derived:

$$\frac{\partial \phi_*}{\partial z}=\alpha\frac{\sigma^2}{g}\phi_* \quad \text{and so} \quad \bar{\phi}_*=\alpha\frac{\sigma^2 h_0}{g}\phi_* \quad \text{at} \quad z=0 \tag{3.9}$$

(b) Boundary condition at impermeable surface

Due to the vanishing of normal velocity to the impermeable surface, it follows that

$$\frac{\partial \phi_*}{\partial \nu}=0 \quad \text{and so} \quad \bar{\phi}_*=0 \quad \text{on impermeable surface} \tag{3.10}$$

Above-mentioned conditions are for fixed boundaries. For moving boundaries in oscillatory motion, similar relations to the above are easily derived.

## IV Formulation for permeable breakwater with sloped-faces

Suppose that a rubble-mound breakwater is located on the impermeable sea bed with wave-side depth $h$ and lee-side depth $h'$, as shown in Fig. 1 and that a sinusoidal wave with

amplitude $\zeta_0$ and frequency $\sigma$ incidents to the breakwater from the right-hand side. The fluid region is divided into five regions, where the first region (I) and the fifth one (V) are to the right of the vertical geometrical furface CB and to the left of vertical surface B'C', respectively. The second region (II) and the fourth region (IV) are those enclosed by CABC and A'C'B'A', respectively. The third one (III) is the region of porous material, enclosed by AA'B'BA.

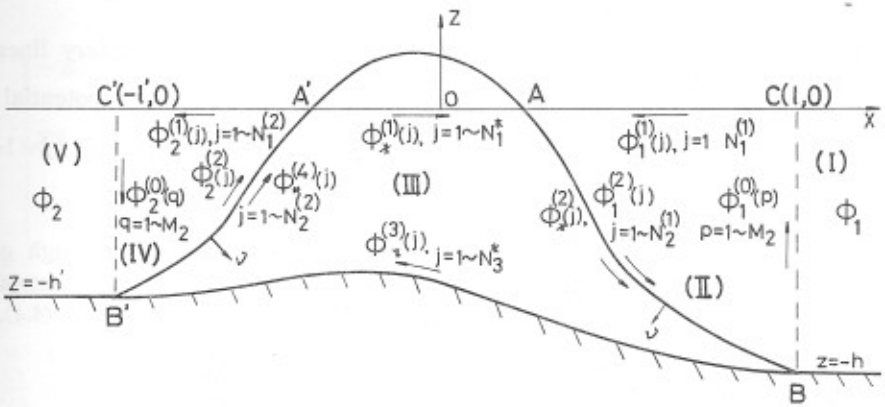


Fig. 1. Definition Sketch for Permeable Sloped-Face Breakwater

(i) Potential functions in the first and fifth regions

Potential function $\varphi_1(x, z)$ in the first region with constant water depth $h$ is expressed as follows:

$$\varphi_1(x,z)=\{e^{ik(x-l)}+A_0e^{-ik(x-l)}\}\frac{\cosh k(z+h)}{\cosh kh}+\sum_{m=1}^{\infty}A_m e^{-k_m(x-l)}\frac{\cos k_m(z+h)}{\cos k_m h} \tag{4.1}$$

where $l$ is the horizontal distance of surface CB from origin O, and $k$ and $k_m$ are the roots of the following equation:

$$kh\tanh kh=-k_m h\tan k_m h=\frac{\sigma^2 h}{g} \qquad (m \text{ is integer}) \tag{4.2}$$

The first term in Eq. (4.1) is the potential function of the incident wave, the second term is that of reflected wave and the last series-terms represent scattering terms. Then, it follows that on the geometrical surface CB the potential function and its normal derivatives to positive $x$-direction at $x=l$ are given as follows:

$$\varphi_1(l,z)=(1+A_0)\frac{\cosh k(z+h)}{\cosh kh}+\sum_{m=1}^{\infty}A_m\frac{\cos k_m(z+h)}{\cos k_m h} \tag{4.3}$$

$$\bar{\varphi}_1(l,z)=\frac{\partial\varphi_1}{\partial(x/h_0)}=\left[ikh(1-A_0)\frac{\cosh k(z+h)}{\cosh kh}-\sum_{m=1}^{\infty}A_m k_m h\frac{\cos k_m(z+h)}{\cos k_m h}\right]\cdot\frac{h_0}{h} \tag{4.4}$$

Similarly, the potential function in the fifth region and its value and normal derivative to negative $x$-direction at $x=-l'$ are given as follows:

$$\varphi_2(x,z)=B_0e^{ik'(x+l')}\frac{\cosh k'(z+h')}{\cosh k'h'}+\sum_{n=1}^{\infty}B_n e^{k_n'(x+l')}\frac{\cos k_n'(z+h')}{\cos k_n'h'} \tag{4.5}$$

$$\varphi_2(-l',z)=B_0\frac{\cosh k'(z+h')}{\cosh k'h'}+\sum_{n=1}^{\infty}B_n\frac{\cos k_n'(z+h')}{\cos k_n'h'} \tag{4.6}$$

$$\bar{\varphi}_2(-l',z)=-\frac{h_0}{h'}\left[iB_0k'h'\frac{\cosh k'(z+h')}{\cosh k'h'}+\sum_{n=1}^{\infty}B_n k_n'h'\frac{\cosh k_n'(z+h')}{\cos k_n'h'}\right] \tag{4.7}$$

where $k'$ and $k_n'$ are the roots of next equations.

$$k'h' \tanh k'h' = -k_n'h' \tan k_n'h' = \frac{\sigma^2 h'}{g} \qquad (n \text{ is integer}) \tag{4.8}$$

The first term in Eq. (4.5) represents the potential function of transmitted wave.

(ii) Potential functions and Green's identity formula in the second region

In the second region, the potential function is denoted by $\phi_1$. The boundary lines $\overrightarrow{CA}$, $\overrightarrow{AB}$ and $\overrightarrow{BC}$ are divided into $N_1^{(1)}$, $N_2^{(1)}$ and $M_1$ segments, respectively and potential functions on these segments are indicated by $\phi_1^{(1)}(j)$ $(j=1\sim N_1^{(1)})$ on $\overrightarrow{CA}$, by $\phi_1^{(2)}(j)$ $(j=1\sim N_2^{(1)})$ on $\overrightarrow{AB}$ and $\phi_1^{(0)}(p)$ $(p=1\sim M_1)$ on $\overrightarrow{BC}$, respectively.

On the boundary $\overrightarrow{BC}$, due to the continuity of mass and energy flux through geometrical surface $BC$ between the first and second fluid regions, it follows, taking the outward normal to the boundary, $\varphi_1(l, z)=\bar{\phi}_1^{(0)}(z)$ and $\varphi_1(l, z)=\phi_1^{(0)}(z)$. Hence, from Eq. (4.3) (4.4),

$$\frac{h_0}{h}\cdot\left[i(1-A_0)\lambda_0 \frac{\cosh k(z+h)}{\cosh \lambda_0} - \sum_{m=1}^{\infty} A_m\lambda_m \frac{\cos k_m(z+h)}{\cos \lambda_m}\right] = \bar{\phi}_1^{(0)}(z) \tag{4.9}$$

$$(1+A_0)\frac{\cosh k(z+h)}{\cosh \lambda_0} + \sum_{m=1}^{\infty} A_m \frac{\cos k_m(z+h)}{\cos \lambda_m} = \phi_1^{(0)}(z) \tag{4.10}$$

where $\lambda_0=kh$ and $\lambda_m=k_mh$.

Multiplying Eq. (4.9) by $\cosh k(z+h)$ or $\cos k_m(z+h)$ and integrating from $z=-h$ to $z=0$, it follows that $A_0$ and $A_m$ are represented by $\bar{\phi}_1^{(0)}$ as follows:

$$A_0 = 1 + \frac{i}{N_0 \sinh \lambda_0} \sum_{p=1}^{M_1} \bar{\phi}_1^{(0)}(p) \cosh k(z_p+h)\cdot\left(\frac{\Delta z_p}{h_0}\right) \tag{4.11}$$

$$A_m = -\frac{1}{N_m \sin \lambda_m} \sum_{p=1}^{M_1} \bar{\phi}_1^{(0)}(p) \cos k_m(z_p+h)\cdot\left(\frac{\Delta z_p}{h_0}\right) \tag{4.12}$$

where $\Delta z_p = \frac{1}{2}(z_{p+1}-z_{p-1})$ and

$$N_0 = \frac{1}{2}\left(1+\frac{2\lambda_0}{\sinh 2\lambda_0}\right), \quad N_m = \frac{1}{2}\left(1+\frac{2\lambda_m}{\sin 2\lambda_m}\right) \tag{4.13}$$

Substituting $A_0$ and $A_m$ into Eq. (4.10), $\phi_1^{(0)}$ is represented by $\bar{\phi}_1^{(0)}$ as follows:

$$\phi_1^{(0)}(p) = 2\frac{\cosh k(z+h)}{\cosh \lambda_0} + \sum_{r=1}^{M_1} f(r:p)\cdot\bar{\phi}_1^{(0)}(r)\cdot\left(\frac{\Delta z_r}{h_0}\right) \tag{4.14}$$

where

$$f(r:p) = i\frac{\cosh k(z_r+h)\cosh k(z_p+h)}{N_0 \sinh \lambda_0 \cosh \lambda_0} - \sum_{m=1}^{\infty} \frac{\cos k_m(z_r+h)\cos k_m(z_p+h)}{N_m \sin \lambda_m \cos \lambda_m} \tag{4.15}$$

and $r$ is used as flowing coordinate on $\overrightarrow{BC}$ in the same manner as $p$.

On the free surface $\overrightarrow{CA}$, $\phi_1^{(1)}(j)$ and $\bar{\phi}_1^{(1)}(j)$ are related by Eq. (3.3).

Applying the Green's identity formula (2.3) to the second region, it follows that at each point $(i)$ on the boundary, the following equation is provided:

$$-\phi(i)+\sum_{j=1}^{N_1^{(1)}}\left(\bar{E}_{ij}^{(1,1)}-\frac{\sigma^2 h_0}{g}E_{ij}^{(1,1)}\right)\phi_1^{(1)}(j)+\sum_{j=1}^{N_2^{(1)}}\left(\bar{E}_{ij}^{(1,2)}\phi_1^{(2)}(j)-E_{ij}^{(1,2)}\bar{\phi}_1^{(2)}(j)\right)$$

$$+\sum_{r=1}^{M_1}F(i,r)\cdot\phi_1^{(1)}(r)=-2\sum_{r=1}^{M_1}\bar{E}_{ir}\frac{\cosh k(z_r+h)}{\cosh\lambda_0} \tag{4.16}$$

Above equation is rewritten, according to the location of point $(i)$ on the boundary, as follows:

$$\sum_{j=1}^{N_1^{(1)}}\begin{Bmatrix}-\delta_{ij}-\dfrac{\sigma^2 h_0}{g}E_{ij}^{(1,1)}\\ \bar{E}_{ij}^{(1,1)}-\dfrac{\sigma^2 h_0}{g}E_{ij}^{(1,1)}\\ \bar{E}_{pj}^{(1,1)}-\dfrac{\sigma^2 h_0}{g}E_{pj}^{(1,1)}\end{Bmatrix}\phi_1^{(1)}(j)+\sum_{j=1}^{N_2^{(1)}}\begin{Bmatrix}\bar{E}_{ij}^{(1,2)}\\ -\delta_{ij}+\bar{E}_{ij}^{(1,2)}\\ \bar{E}_{pj}^{(1,2)}\end{Bmatrix}\phi_1^{(2)}(j)-\sum_{j=1}^{N_2^{(1)}}\begin{Bmatrix}E_{ij}^{(1,2)}\\ \text{〃}\\ E_{pj}^{(1,2)}\end{Bmatrix}\bar{\phi}_1^{(2)}(j)$$

$$+\sum_{r=1}^{M_1}\begin{Bmatrix}F(i,r)\\ \text{〃}\\ -G(p,r)\end{Bmatrix}\bar{\phi}_1^{(0)}(r)=2\times\begin{cases}-\sum_{r=1}^{M_1}\bar{E}_{ir}\dfrac{\cosh k(z_r+h)}{\cosh\lambda_0} & \cdots\cdots i=1\sim N_1^{(1)} \quad (4.17)\\ \text{〃} & \cdots\cdots i=1\sim N_2^{(1)} \quad (4.18)\\ \dfrac{\cosh k(z_p+h)}{\cosh\lambda_0} & \cdots\cdots i=p=1\sim M_1 \quad (4.19)\end{cases}$$

where $\delta_{ij}$ is Kronecker's delta, that is, $\delta_{ij}=1$ $(i=j)$ : $=0$ $(i\neq j)$. And

$$F(i,r)=\sum_{p=1}^{M_1}\bar{E}_{ip}f(r:p)\cdot\frac{\Delta z_r}{h_0}-E_{ir},\quad G(p,r)=f(r:p)\frac{\Delta z_r}{h_0}+E_{pr} \tag{4.20}$$

(iii) Potential functions and Green's identity formula in the fourth region

In the fourth region, the potential function is denoted by $\phi_2$ and the boundary lines $\overrightarrow{A'C'}$, $\overrightarrow{C'B'}$ and $\overrightarrow{B'A'}$ are divided into $N_1^{(2)}$, $M_2$ and $N_2^{(2)}$ segments, respectively, where potential functions are indicated by $\phi_2^{(1)}(j)$ $(j=1\sim N_1^{(2)})$, $\phi_2^{(0)}(q)$ $(q=1\sim M_2)$ and $\phi_2^{(2)}(j)$ $(j=1\sim N_2^{(2)})$, respectively.

Similarly to the second region, taking the outward normal to the boundary, $B_0$, $B_n$ and $\phi_2^{(0)}$ are represented by $\bar{\phi}_2^{(0)}$ as follows:

$$B_0=\frac{i}{N_0'\sinh\lambda_0'}\sum_{q=1}^{M_2}\bar{\phi}_2^{(0)}(q)\cosh k'(z_q+h')\cdot\left|\frac{\Delta z_q}{h_0}\right| \tag{4.21}$$

$$B_n=-\frac{1}{N_n'\sin\lambda_n'}\sum_{q=1}^{M_2}\bar{\phi}_2^{(0)}(q)\cos k_n'(z_q+h')\cdot\left|\frac{\Delta z_q}{h_0}\right| \tag{4.22}$$

$$\phi_2^{(0)}(q)=\sum_{s=1}^{M_2}f'(s:q)\bar{\phi}_2^{(0)}(s)\cdot\left|\frac{\Delta z_s}{h_0}\right| \tag{4.23}$$

where

$$f'(s:q)=i\frac{\cosh k'(z_s+h')\cosh k'(z_q+h')}{N_0'\sinh\lambda_0'\cosh\lambda_0'}-\sum_{n=1}^{\infty}\frac{\cos k_n'(z_s+h')\cos k_n'(z_q+h')}{N_n'\sin\lambda_n'\cos\lambda_n'} \tag{4.24}$$

$$\lambda_0'=k'h',\quad \lambda_n'=k_n'h',\quad N_0'=\frac{1}{2}\left(1+\frac{2\lambda_0'}{\sinh 2\lambda_0'}\right),\quad N_n'=\frac{1}{2}\left(1+\frac{2\lambda_n'}{\sin 2\lambda_n'}\right) \tag{4.25}$$

and $s$ is the flowing coordinate on $C'B'$ in the same manner as $q$.

The Green's identity formula to the fourth region is as follows:

$$-\phi_2(i)+\sum_{j=1}^{N_1^{(2)}}(\bar{E}_{ij}^{(2,1)}-\frac{\sigma^2 h_0}{g}E_{ij}^{(2,1)})\,\phi_2^{(1)}(j)+\sum_{j=1}^{N_2^{(2)}}(\bar{E}_{ij}^{(2,2)}\phi_2^{(2)}(j)$$

$$-E_{ij}^{(2,2)}\bar{\phi}_2^{(2)}(j))+\sum_{s=1}^{M_2}F'(i,s)\,\bar{\phi}_2^{(0)}(s)=0 \tag{4.26}$$

Above equation is rewritten, according to the location of point $(i)$, as follows:

$$\sum_{j=1}^{N_1^{(2)}}\begin{Bmatrix}-\delta_{ij}-\frac{\sigma^2 h_0}{g}E_{ij}^{(2,1)}\\ \bar{E}_{ij}^{(2,1)}-\frac{\sigma^2 h_0}{g}E_{ij}^{(2,1)}\\ \bar{E}_{qj}^{(2,1)}-\frac{\sigma^2 h_0}{g}E_{qj}^{(2,1)}\end{Bmatrix}\phi_2^{(1)}(j)+\sum_{j=1}^{N_2^{(2)}}\begin{Bmatrix}\bar{E}_{ij}^{(2,2)}\\ -\delta_{ij}+\bar{E}_{ij}^{(2,2)}\\ \bar{E}_{qj}^{(2,2)}\end{Bmatrix}\phi_2^{(2)}(j)$$

$$-\sum_{j=1}^{N_2^{(2)}}\begin{Bmatrix}E_{ij}^{(2,2)}\\ \#\\ E_{qj}^{(2,2)}\end{Bmatrix}\bar{\phi}_2^{(2)}(j)+\sum_{s=1}^{M_2}\begin{Bmatrix}F'(i,s)\\ \#\\ -G'(q,s)\end{Bmatrix}\bar{\phi}_2^{(0)}(s)=0\quad\begin{matrix}\cdots\cdots\ i=1\sim N_1^{(2)}\\ \cdots\cdots\ i=1\sim N_2^{(2)}\\ \cdots\cdots\ i=q=1\sim M_2\end{matrix}\tag{4.27, 4.28, 4.29}$$

where

$$F'(i,s)=\sum_{q=1}^{M_2}\bar{E}_{iq}f'(s:q)\cdot\left|\frac{\Delta z_s}{h_0}\right|-E_{is},\quad G'(q,s)=f'(s:q)\cdot\left|\frac{\Delta z_s}{h_0}\right|+E_{qs} \tag{4.30}$$

(iv) Potential functions and Green's identity formula in the third region

Potential function in the third region is denoted by $\phi_*$ and boundary lines $\overrightarrow{A'A}$, $\overrightarrow{AB}$, $\overrightarrow{BB'}$ and $\overrightarrow{B'A'}$ are divided into $N_1{}^*$, $N_2{}^{(1)}$, $N_3{}^*$ and $N_2{}^{(2)}$ segments, where potential functions are indicated by $\phi_*^{(1)}(j)$ $(j=1\sim N_1{}^*)$, $\phi_*^{(2)}(j)$ $(j=1\sim N_2{}^{(1)})$, $\phi_*^{(3)}(j)$ $(j=1\sim N_3{}^*)$ and $\phi_*^{(4)}(j)$ $(j=1\sim N_2{}^{(2)})$, respectively. And the normal to the boundary is taken inward.

On the free boundary $\overrightarrow{A'A}$, $\bar{\phi}_*$ and $\phi_*$ are related as follows, on account of Eq. (3.9) and of inward normal:

$$\bar{\phi}_*^{(1)}=-\alpha\cdot\frac{\sigma^2 h_0}{g}\phi_*^{(1)} \tag{4.31}$$

On the impervious boundary $\overrightarrow{BB'}$, $\bar{\phi}_*^{(3)}(j)$ vanishes identically.

On the boundaries $\overrightarrow{AB}$ and $\overrightarrow{B'A'}$, due to the continuity of mass and energy flux, it follows that

$$\beta\phi_*^{(2)}=\phi_1^{(2)},\ \bar{\phi}_*^{(2)}=\bar{\phi}_1^{(2)}\quad\text{and}\quad\beta\phi_*^{(4)}=\phi_2^{(2)},\ \bar{\phi}_*^{(4)}=\phi_2^{(2)} \tag{4.32}$$

On account of above conditions, Green's identity formula in the third region becomes as follows:

$$\phi_*(i)+\sum_{j=1}^{N_1^*}(\bar{E}_{ij}^{*(1)}+\alpha\frac{\sigma^2 h_0}{g}E_{ij}^{(1)})\,\phi_*^{(1)}(j)+\sum_{j=1}^{N_2^{(1)}}(\frac{1}{\beta}\bar{E}_{ij}^{*(2)}\phi_1^{(2)}(j)-E_{ij}^{*(2)}\bar{\phi}_1^{(2)}(j))$$

$$+\sum_{j=1}^{N_3^*}\bar{E}_{ij}^{*(3)}\phi_*^{(3)}(j)+\sum_{j=1}^{N_2^{(2)}}(\frac{1}{\beta}\bar{E}_{ij}^{*(4)}\phi_2^{(2)}(j)-E_{ij}^{*(4)}\bar{\phi}_2^{(2)}(j))=0 \tag{4.33}$$

According to the location of the point $(i)$, the first term $\phi_*(i)$ should be written as follows:

$$\begin{aligned}
&\text{For point } (i) \text{ on } \overrightarrow{A'A}\ (i=1\sim N_1^*): \quad \phi_*(i)=\phi_*^{(1)}(i), \quad \bar{E}_{ij}^{*(1)}=0\\
&\quad\ \ \text{//}\quad\ \ \text{//}\quad\ \ \overrightarrow{AB}\ (i=1\sim N_1^{(2)}): \quad \phi_*(i)=\frac{1}{\beta}\phi_1^{(2)}(i)\\
&\quad\ \ \text{//}\quad\ \ \text{//}\quad\ \ \overrightarrow{BB'}\ (i=1\sim N_3^*): \quad \phi_*(i)=\phi_*^{(3)}(i)\\
&\quad\ \ \text{//}\quad\ \ \text{//}\quad\ \ \overrightarrow{B'A'}\ (i=1\sim N_2^{(2)}): \quad \phi_*(i)=\frac{1}{\beta}\phi_2^{(2)}(i)
\end{aligned} \tag{4.34}$$

(v) Determination of potential functions on the boundaries

Eq. (4.17)~(4.19), Eq. (4.27)~(4.29) and Eq. (4.33) provide linear equations with respect to potential functions on the boundaries. They are $(N_1^{(1)}+2N_2^{(1)}+N_1^{(2)}+2N_2^{(2)}+N_1^*+N_3^*+M_1+M_2)$ equations with respect to the same number of unknowns $\phi_1^{(1)}$, $\phi_1^{(2)}$, $\phi_1^{(2)}$, $\phi_2^{(1)}$, $\phi_2^{(2)}$, $\phi_2^{(2)}$, $\phi_*^{(1)}$, $\phi_*^{(2)}$ and $\phi_1^{(0)}$, $\phi_2^{(0)}$. Consequently, by solving these equations, simultaneously, all of unknowns are determined, from which $A_0$, $A_m$ and $B_0$, $B_n$ are obtained by Eq. (4.11) (4.12) and Eq. (4.21) (4.22) and potential functions at an interior point $(x, z)$ in every fluid region are calculated by Eq. (2.5) and Eq. (4.1) (4.5).

In above equations, $E_{ij}$ and $\bar{E}_{ij}$ are calculated numerically as follows:

$$\begin{aligned}
&E_{ij}=\frac{1}{\pi}\log(R_{ij}/h_0)\cdot\frac{\Delta S_j}{h_0}, \quad E_{ii}=\frac{1}{\pi}\left(\log\frac{\Delta S_i/h_0}{2}-1\right)\cdot\frac{\Delta S_i}{h_0}\\
&\bar{E}_{ij}=\frac{1}{\pi R_{ij}}\left(\frac{\xi_j-\xi_i}{R_{ij}}\Delta\eta_j-\frac{\eta_j-\eta_i}{R_{ij}}\Delta\xi_j\right), \quad \bar{E}_{ii}=\frac{1}{2\pi}(\xi_s\eta_{ss}-\eta_s\xi_{ss})_i\cdot\Delta S_i\\
&\xi_s=\frac{\xi_{i+1}-\xi_{i-1}}{2\Delta S_i}, \quad \xi_{ss}=\frac{6}{\Delta S_{i+1}+\Delta S_i+\Delta S_{i-1}}\left(\frac{\xi_{i+1}-\xi_i}{\Delta S_{i+1}+\Delta S_i}-\frac{\xi_i-\xi_{i-1}}{\Delta S_i+\Delta S_{i-1}}\right)\\
&\Delta S_j=\sqrt{(\Delta\xi_j)^2+(\Delta\eta_j)^2}, \quad \Delta\xi_j=\frac{1}{2}(\xi_{j+1}-\xi_{j-1}), \quad \Delta\eta_j=\frac{1}{2}(\eta_{j+1}-\eta_{j-1})
\end{aligned} \tag{4.35}$$

$\eta_s$ and $\eta_{ss}$ are shown by replacing $\xi$ by $\eta$ in above expressions.

(vi) Wave transformation

The reflection and transmission coefficients $K_r$ and $K_t$ by breakwater are provided as follows:

$$K_r=|A_0| \quad \text{and} \quad K_t=|B_0| \tag{4.36}$$

And also, on account of the continuity of energy flux through breakwater, it follows that the coefficient of energy loss in breakwater is calculated as

$$K_l^2=1-K_r^2-\frac{N_0'\lambda_0}{N_0\lambda_0'}\cdot\frac{h'}{h}\cdot K_t^2 \tag{4.37}$$

Wave height distribution around breakwater is calculated as follows:

$$\begin{aligned}
&(1)\ \text{From } -\infty \text{ to point } C': \quad \left|\frac{\zeta_0^{(2)}}{\zeta_0}\right|=\left|B_0e^{ik'(x+l')}+\sum_{n=1}^{\infty}B_ne^{k_n'(x+l')}\right|\\
&(2)\ \text{From point } C' \text{ to } A': \quad \left|\frac{\zeta^{(2)}}{\zeta_0}\right|=\left|\phi_2^{(1)}(j)\right| \qquad (j=N_1^{(2)}\sim 1)\\
&(3)\ \text{From point } A' \text{ to } A: \quad \left|\frac{\zeta_*}{\zeta_0}\right|=\left|\beta\phi_*^{(1)}(j)\right| \qquad (j=1\sim N_1^*)
\end{aligned} \tag{4.38}$$

(4) From point $A$ to $C$ : $\left|\frac{\zeta^{(1)}}{\zeta_0}\right| = \left|\phi_1{}^{(1)}(j)\right| \qquad (j=N_1{}^{(1)}\sim 1)$

(5) From point $C$ to : $\left|\frac{\zeta_0{}^{(1)}}{\zeta_0}\right| = \left|e^{ik(x-l)} + A_0 e^{-ik(x-l)} + \sum_{m=1}^{\infty} A_m e^{-k_m(x-l)}\right|$

(vii) Vertical-face breakwater

For vertical-face breakwater as shown in Fig. 2, the Green's identity formula applied to the fluid region ABB'A' of permeable breakwater provides the following equations with respect to potential functions on the boundaries :

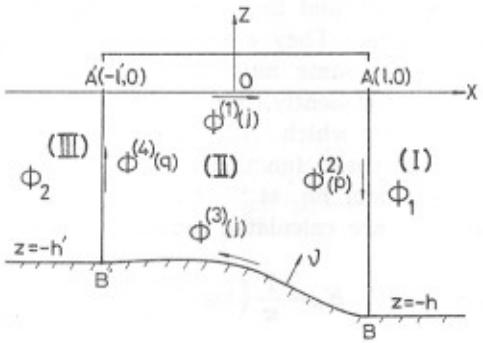


Fig. 2. Definition Sketch for Permeable Vertical-Face Breakwater

$$\sum_{j=1}^{N_1^*}\begin{Bmatrix}\delta_{ij}+\alpha\cdot\dfrac{\sigma^2 h_0}{g}E_{ij}^{*(1)}\\ \bar{E}_{ij}^{*(1)}+\alpha\dfrac{\sigma^2 h_0}{g}E_{ij}^{*(1)}\\ \bar{E}_{pj}^{*(1)}+\alpha\dfrac{\sigma^2 h_0}{g}E_{pj}^{*(1)}\\ \bar{E}_{qj}^{*(1)}+\alpha\dfrac{\sigma^2 h_0}{g}E_{qj}^{*(1)}\end{Bmatrix}\phi_*^{(1)}(j)+\sum_{j=1}^{N_3^*}\begin{Bmatrix}\bar{E}_{ij}^{*(3)}\\ \delta_{ij}+\bar{E}_{ij}^{*(3)}\\ \bar{E}_{pj}^{*(3)}\\ \bar{E}_{qj}^{*(3)}\end{Bmatrix}\phi_*^{(3)}(j)-\sum_{r=1}^{M_1}\begin{Bmatrix}F_*(i,r)\\ \text{〃}\\ G_*(p,r)\\ F_*(q,r)\end{Bmatrix}\bar{\phi}_*^{(2)}(r)$$

$$-\sum_{s=1}^{M_2}\begin{Bmatrix}F'_*(i,s)\\ \text{〃}\\ F'_*(p,s)\\ G'_*(q,s)\end{Bmatrix}\bar{\phi}_*^{(4)}(s)=-\frac{2}{\beta}\times\begin{cases}\sum_{r=1}^{M_1}\bar{E}_{ir}^{*(2)}\dfrac{\cosh k(z_r+h)}{\cosh\lambda_0} & \cdots\cdots i=1\sim N_1^* \quad (4.39)\\ \text{〃} & \cdots\cdots i=1\sim N_3^* \quad (4.40)\\ \dfrac{\cosh k(z_p+h)}{\cosh\lambda_0} & \cdots\cdots i=p=1\sim M_1 \quad (4.41)\\ \sum_{r=1}^{M_1}\bar{E}_{qr}^{*(2)}\dfrac{\cosh k(z_r+h)}{\cosh\lambda_0} & \cdots\cdots i=q=1\sim M_2 \quad (4.42)\end{cases}$$

where

$$F_*(i,r)=\frac{1}{\beta}\sum_{q=1}^{M_1}\bar{E}_{iq}^{*(2)}f(r:p)\cdot\left|\frac{\Delta z_r}{h_0}\right|+E_{ir}^{*(2)},\quad G_*(p,r)=\frac{1}{\beta}f(r:p)\cdot\left|\frac{\Delta z_r}{h_0}\right|+E_{pr}^{*(2)}$$
$$F'_*(i,s)=\frac{1}{\beta}\sum_{q=1}^{M_2}\bar{E}_{iq}^{*(4)}f'(s:q)\cdot\left(\frac{\Delta z_s}{h_0}\right)+E_{is}^{*(4)},\quad G'_*(q,s)=\frac{1}{\beta}f'(s:q)\cdot\left(\frac{\Delta z_s}{h_0}\right)+E_{qs}^{*(4)} \qquad (4.43)$$

Solving Eq. (4.39)~(4.42), $\phi_*^{(1)}$, $\bar{\phi}_*^{(2)}$, $\phi_*^{(3)}$ and $\bar{\phi}_*^{(4)}$ are determined, from which $\phi_*^{(2)}$, $\phi_*^{(4)}$ and $A_0$, $A_m$, $B_0$, $B_n$ are calculated as follows:

$$\left.\begin{aligned}\phi_*^{(2)}(p) &= \frac{1}{\beta}\left[\frac{2\cosh k(k_p+h)}{\cosh \lambda_0} - \sum_{r=1}^{M_1} f(r:p)\cdot\bar{\phi}_*^{(2)}(r)\cdot\left|\frac{\Delta z_r}{h_0}\right|\right]\\ \phi_*^{(4)}(q) &= -\frac{1}{\beta}\sum_{s=1}^{M_2} f'(s:q)\,\bar{\phi}_*^{(4)}(s)\cdot\left(\frac{\Delta z_s}{h_0}\right)\end{aligned}\right\} \tag{4.44}$$

$$\left.\begin{aligned}A_0 &= 1-\frac{i}{N_0\sinh\lambda_0}\sum_{p=1}^{M_1}\bar{\phi}_*^{(2)}(p)\cosh k(z_p+h)\cdot\left|\frac{\Delta z_p}{h_0}\right|\\ A_m &= \frac{1}{N_m\sin\lambda_m}\sum_{q=1}^{M_1}\bar{\phi}_*^{(2)}(p)\cos k_m(z_p+h)\cdot\left|\frac{\Delta z_p}{h_0}\right|\end{aligned}\right\} \tag{4.45}$$

$$\left.\begin{aligned}B_0 &= \frac{-i}{N_0'\sinh\lambda_0'}\sum_{q=1}^{M_2}\bar{\phi}_*^{(4)}(q)\cosh k'(z_q+h')\cdot\left(\frac{\Delta z_q}{h_0}\right)\\ B_n &= \frac{1}{N_n'\sin\lambda_n'}\sum_{q=1}^{M_2}\bar{\phi}_*^{(4)}(q)\cos k_n'(z_q+h')\cdot\left(\frac{\Delta z_q}{h_0}\right)\end{aligned}\right\} \tag{4.46}$$

Wave transformation is calculated by the same way as (vi).

## V Formulation for sloped-face seawall

Suppose that a seawall of porous materials AB is placed on the impermeable slope DCB as shown in Fig. 3 and a sinusoidal wave incidents from the right. The fluid domain is divided into three regions (I) (II) and (III), similarly to the case of breakwater. The potential functions in these regions are denoted by $\varphi(x, z)$, $\phi$ and $\phi_*$, respectively, and those on boundary lines for each region are indicated as shown in the figure.

$\varphi(x, z)$ in the region (I) is expressed by Eq. (4.1) putting $l=0$, and $A_0$, $A_m$ are given by Eq. (4.11) and (4.12). The Green's identities for the region (II) are entirely the same as Eq. (4.17) (4.18) (4.19) and those for the region (III) are given by Eq. (4.33), dropping the last terms in the lefthand side.

The reflection coefficient is provided by $K_r=|A_0|$, and coefficient of energy loss is by $K_l^2=1-K_r^2$. Wave height distributions in front of seawall are calculated by the same way as Eq. (4.38).

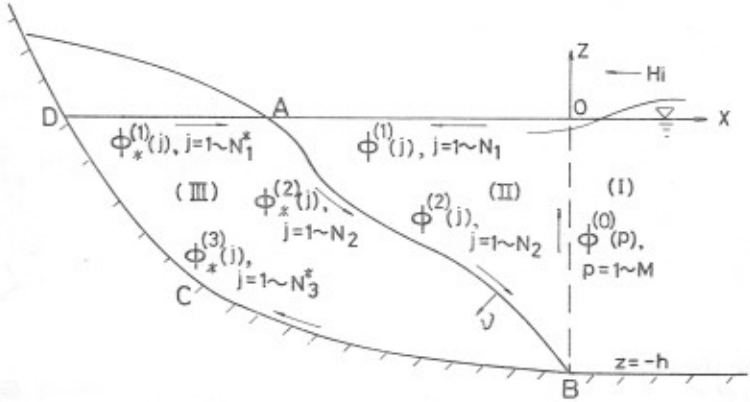


Fig. 3. Definition Sketch for Permeable Sloped-Face Seawall

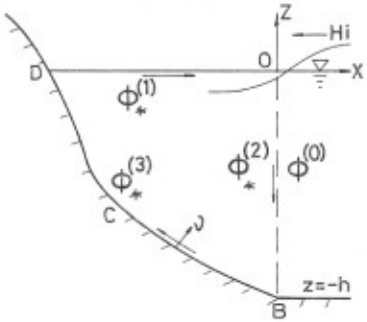


Fig. 4. Definition Sketch for Permeable Vertical-Face Seawall

For the vertical-face seawall when the boundary line AB in Fig. 3 becomes vertical as shown in Fig. 4, the Green's identities for the boundaries DO, BCD and OB are given by Eq. (4.39) (4.40) and (4.41), respectively, dropping the last terms in the left-hand side.

## VI Wave transformation by gradual changes in underwater depth and in beach profiles of impermeable bed

Waves on sloping beach were analyzed by Miche (1944), Friedrichs (1948), Isaacson (1950) and others. Waves on underwater step were analyzed by Newman (1965), Miles (1967) and Ijima (1971).*

The former investigations are purely mathematical and seem to be rather difficult for engineers to apply to practical problems, though they are limitted to the case of uniformely sloping bottom and of small amplitude waves excepting Miche's. The latter investigations are easily applied to practical problems but in actual field it is rare to encounter the underwater step, that is, discontinuous change of water depth.

The wave transformation by irregular or gradual change of water depth and that of beach profiles are easily analyzed numerically as the most simple cases of the proposed method.

(i) Wave transformation by gradual change of water depth

This is treated as the extreme case of Fig. 2 when the breakwater ABB'A' on impervious, gradually varying sea bed BB' disappears. Such a situation is represented by putting $V=1$ and $\mu/\sigma=0$, that is, $\alpha=1$, $\beta=1$ in Eq. (4.39)~(4.46).

(ii) Wave transformation by irregular change of beach profile

This problem is treated as the extreme case of Fig. 3 when the permeable seawall ABCD becomes impervious. This situation is realized by putting the normal derivatives $\phi^{(2)}$ on the boundary AB to be zero. Hence, the Green's identities to be solved are given by Eq. (4.17) (4.19), dropping the third terms of the left-hand sides.

## VII Formulation for submerged breakwater

Suppose that a permeable submerged breakwater CDE is placed on sea bed with wave-side depth $h$ and lee-side depth $h'$ as shown in Fig. 5. In this case, fluid region is divided into four regions by geometrical surface AE and BC. The potential function $\varphi_1(x, z)$, $\varphi_2(x, z)$ in the first and fourth regions (I), (IV) are the same as Eq. (4.1) and (4.5). Those in the second and third regions (II), (III) are denoted by $\phi$ and $\phi_*$, and on the boundaries are by $\phi^{(1)}$, $\phi^{(2)}$, $\phi_1^{(0)}$, $\phi_2^{(0)}$ and $\phi_*^{(1)}$, $\phi_*^{(2)}$ as shown in the figure. Then, the Green's identities for the second region are written as follows:

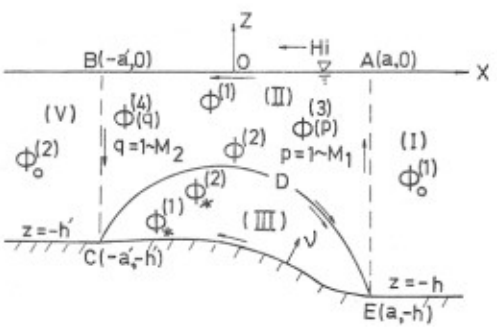


Fig. 5. Definition Sketch for Permeable Submerged Breakwater

$$\sum_{j=1}^{N_1}\begin{Bmatrix} -\delta_{ij}-\dfrac{\sigma^2 h_0}{g}E_{ij}^{(1)} \\ \bar{E}_{ij}^{(1)}-\dfrac{\sigma^2 h_0}{g}E_{ij}^{(1)} \\ E_{pj}^{(1)}-\dfrac{\sigma^2 h_0}{g}E_{pj}^{(1)} \\ \bar{E}_{qj}^{(1)}-\dfrac{\sigma^2 h_0}{g}E_{qj}^{(1)} \end{Bmatrix}\phi^{(1)}(j)+\sum_{j=1}^{N_2}\begin{Bmatrix} \bar{E}_{ij}^{(2)} \\ -\delta_{ij}+\bar{E}_{ij}^{(2)} \\ \bar{E}_{pj}^{(2)} \\ \bar{E}_{qj}^{(2)} \end{Bmatrix}\phi^{(2)}(j)$$

$$-\sum_{j=1}^{N_2}\begin{Bmatrix} E_{ij}^{(2)} \\ // \\ E_{pj}^{(2)} \\ E_{qj}^{(2)} \end{Bmatrix}\bar{\phi}^{(2)}(j)+\sum_{r=1}^{M_1}\begin{Bmatrix} F(i,r) \\ // \\ -G(y,r) \\ F(q,r) \end{Bmatrix}\bar{\phi}_1{}^{(0)}(r)+\sum_{s=1}^{M_2}\begin{Bmatrix} F'(i,s) \\ // \\ F'(p,s) \\ -G'(q,s) \end{Bmatrix}\bar{\phi}_2{}^{(0)}(s)$$

$$= 2\times\begin{cases} -\sum_{r=1}^{M_1}\bar{E}_{ir}\dfrac{\cosh k(z_r+h)}{\cosh\lambda_0} & \cdots\cdots i=1\sim N_1 \quad (7.1) \\ // & \cdots\cdots i=1\sim N_2 \quad (7.2) \\ \dfrac{\cosh k(z_p+h)}{\cosh\lambda_0} & \cdots\cdots i=p=1\sim M_1 \quad (7.3) \\ -\sum_{r=1}^{M_1}\bar{E}_{qr}\dfrac{\cosh k(z_r+h)}{\cosh\lambda_0} & \cdots\cdots i=q=1\sim M_2 \quad (7.4) \end{cases}$$

where $F(i, r)$, $G(p, r)$ and $F'(i, s)$, $G'(q, s)$ are given by Eq. (4.20) and (4.30), respectively.

The Green's identities for the third region are provided as follows:

$$\sum_{j=1}^{N_1{}^*}\begin{Bmatrix} \delta_{ij}+\bar{E}_{ij}^{*(1)} \\ \bar{E}_{ij}^{*(1)} \end{Bmatrix}\phi_*^{(1)}(j)+\sum_{j=1}^{N_2}\begin{Bmatrix} \dfrac{1}{\beta}E_{ij}^{*(2)} \\ \dfrac{1}{\beta}(\delta_{ij}+\bar{E}_{ij}^{*(2)}) \end{Bmatrix}\phi^{(2)}(j)$$

$$-\sum_{j=1}^{N_2}\begin{Bmatrix} E_{ij}^{*(2)} \\ // \end{Bmatrix}\bar{\phi}^{(2)}(j)=0 \qquad \begin{matrix} \cdots\cdots i=1\sim N_1{}^* & (7.5) \\ \cdots\cdots i=1\sim N_2 & (7.6) \end{matrix}$$

Solving Eq. (7.1)$\sim$(7.6), simultaneously, potential functions on the boundaries are determined, from which $A_0$, $A_m$, $B_0$, $B_n$ in $\varphi_1(x, z)$ and $\varphi_2(x, z)$ are calculated by Eq. (4.11) (4.12) and (4.21) (4.22). Wave transformations are calculated in the same way as Eq. (4.38), and the horizonal and vertical wave forces $F_x$ and $F_z$ for the submerged breakwater are calculated as follows:

$$\left.\begin{aligned} \left|\frac{F_x}{\rho g\zeta_0 h}\right| &= \left|\sum_{j=1}^{N_2}\phi^{(2)}(j)\frac{\Delta\eta_j}{h}+\beta\sum_{j=1}^{N_1{}^*}\phi_*^{(1)}(j)\frac{\Delta\eta_j}{h}\right| \\ \left|\frac{F_z}{\rho g\zeta_0 h}\right| &= \left|\sum_{j=1}^{N_2}\phi^{(2)}(j)\frac{\Delta\xi_j}{h}+\beta\sum_{j=1}^{N_1{}^*}\phi_*^{(1)}(j)\frac{\Delta\xi_j}{h}\right| \end{aligned}\right\} \qquad (7.7)$$

## VII Calculations and Results

(i) Permeable breakwater with sloped-faces

We consider four types of cross-sections as shown in Fig. 6 (a) (b) (c) (d). In the first three types the width of breakwater at still water level B is equal to the water depth $h$ and the slopes of both faces are 1 : 1.5. The type A is the case when above cross-section is placed on the constant water depth $h$. The type B is the one with fore-side depth $h$ and rearside depth 0.5h. The type C is the case when the breakwater has an impermeable core whose face-slope is 1 : 1.5 and whose upper surface of width 0.6h is at the depth of 0.4h from still water surface. The last type D has the width B = 1.6h and side slope 1 : 1.3.

The number of calculation points on each boundary line is shown in the figure. In calculations, the series terms in Eq. (4.1) and (4.5) are taken from $m=1$ to $m=9$ and from $n=1$ to $n=9$, respectively. The porosity $V$ is taken as 0.5 and coefficient of resistance $\mu/\sigma$ as 1.0. For type D, the case when $V=0.4$ and $\mu/\sigma=0.5$ is also calculated.

Fig. 7(a) shows the calculated reflection-, transmission- and energy loss-coefficient $K_r$, $K_t$ and $K_l$ for types A, B and C. From these figures, it is found that for waves with $\sigma^2 h/g$ larger than 1.5 there is almost no difference among calculated values for the three types but for waves with $\sigma^2 h/g$ smaller than 1.5 appears some difference. Due to the effect of bottom slope in type B and of the core in type C, the reflection coefficients for B and C are larger than those for A, and the transmission coefficients for them are larger or smaller than those for A, according to the values of $\sigma^2 h/g$. From the energy loss coefficient, it is seen that the wave absorbing ability becomes lower in the order of A, B and C, according to the cross-sectional areas of permeable materials in three types.

Fig. 7(b) is the calculated values for type D, where it is seen that for $V=0.5$ and $\mu/\sigma=1.0$ the reflection and transmission coefficients are smaller than those for above three types, due to larger cross-sectional area. For $V=0.4$ and $\mu/\sigma=0.5$, both of reflection and transmission coefficients are larger than when $V=0.5$ and $\mu/\sigma=1.0$.

According to the author's investigation on permeable vertical breakwater (1971), the decrease (or increase) in porosity $V$ causes the increase (or decrease) of reflection coefficient but does not so largely affect the transmission coefficient, while decrease (or increase) in resistance $\mu/\sigma$ causes remarkable increase (or decrease) of transmission coefficient but does not so largely affect the reflection coefficient. In the same way as above, it is considered that the decrease of porosity $V$ from 0.5 to 0.4 results in the increase of reflection coefficient and that of resistance $\mu/\sigma$ from 1.0 to 0.5 causes the increase of transmission coefficient.

In the figure, the measured values for incident wave steepness $H_0/L \approx 0.03$ by the experiment of Hattori and Sakai (1973) with the same cross-section as the type D are plotted for reference. In their experiment, water depth $h$ is 38.1 cm, width of breakwater at still water level B is 61.4 cm and breakwater model is made of $7.8 \times 9.3$ cm motar blocks and the porosity is 0.5. The calculated values disagree with experiment for large $\sigma^2 h/g$.

In order to express reasonably the tendency of $K_r$ and $K_t$ in relation to $\sigma^2 h/g$, it is necessary to present the numerical values of $V$ and $\mu/\sigma$ as functions of $\sigma^2 h/g$. Sollitt (1972), Madson (1973) and others estimated the value of $\mu/\sigma$ by means of stationary flow resistance and of the Lorentz's equivalent work assumption in porous material. But, in addition, the porosity $V$ including the effect of virtual mass coefficient should also be estimated in any way. However, such an estimation for $V$ and $\mu/\sigma$ are not yet established at present.

After the author's investigation (1971), it seems that the reasonable value of $\mu/\sigma$ is about 1.0 for $\sigma^2 h/g = 1.0$, lager than 1.0 for $\sigma^2 h/g < 1.0$ and smaller than 1.0 for $\sigma^2 h/g > 1.0$. And $V$ is to be taken as smaller than actual porosity. In the calculations of this

paper, $V$ and $\mu/\sigma$ are kept constant independently on $\sigma^2 h/g$, for convenience. (It should be noticed that breaking of waves on sloped-face should depress the reflection and transmission but such an effect is ignored here.)

The wave height distribution around the breakwater of type A, C and D are calculated by Eq. (4.38) and shown in Fig. 8(a) (b) (c). It is seen that in every type the low height of waves (node) appears on the foreside face, then the wave height increases abruptly nearby the water line of the face and decreases exponentially in porous breakwater. It is characteristic that the transmission- and energy loss-coefficient for type A and D are nearly equal in spite of the remarkable difference in breakwater width between them. This suggests that the wave absorbing ability of permeable solped-face breakwater will not increase as the increase of breakwater width beyond certain limit.

Also, it is clear that the reflection- and transmission-coefficient of the type C are fairly large for small $\sigma^2 h/g$, compared with those of type A, and so the wave absorbing ability becomes lower due to the existence of impermeable core.

Fig. 9(a)(b)(c)(d) are the distributions of velocity potentials around breakwater of type A calculated by Eq. (2.5) (4.1) (4.5) for wave of $\sigma^2 h/g=0.6$, where full lines are equipotential lines and broken lines are orthogonals to them. (a) is those at $\sigma t=0°$, (b) is at $\sigma t=30°$, (c) is at $\sigma t=60°$ and (d) is at $\sigma t=90°$. Fig. 10(a)(b)(c)(d) are the same as above for type C breakwater for wave of $\sigma^2 h/g=0.6$. From these figures we can see the time history of flow pattern in permeable breakwater and it is found that the flow in porous body of type A breakwater concentrates upwards at the still water level through the body and the point of concentration progresses as the wave crest approaches to the breakwater. The flow pattern for type C breakwater is similar to the above but concentration of flow to the water surface through porous material is more remarkable, due to impermeable core. Such a figure of flow pattern will be used effectively in interpretation of breakwater disaster.

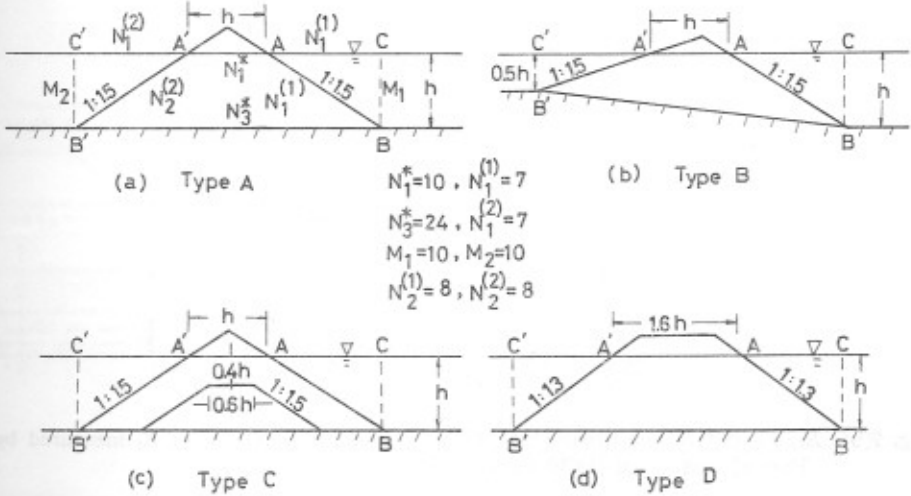


Fig. 6. (a) (b) (c) (d) Calculated Cross-Section of Permeable Breakwater of Sloped Faces

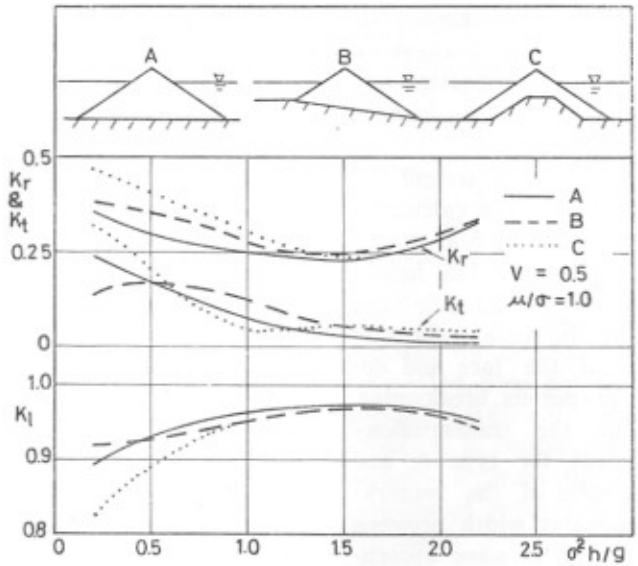


Fig. 7(a) $K_r$, $K_t$ and $K_l$ for Breakwater with Sloped-Faces

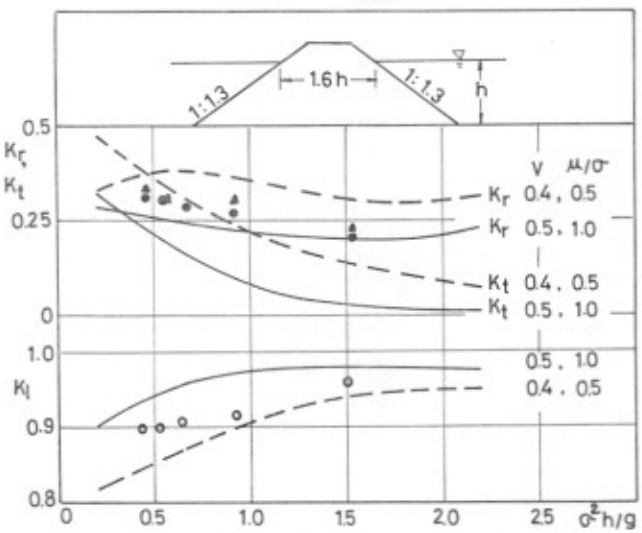


Fig. 7(b) $K_r$, $K_t$ and $K_l$ for Breakwater with Sloped-Faces (•: $K_r$, ▲: $K_t$ measured by Hattori and Sakai (1970) for $H/L=0.03$)

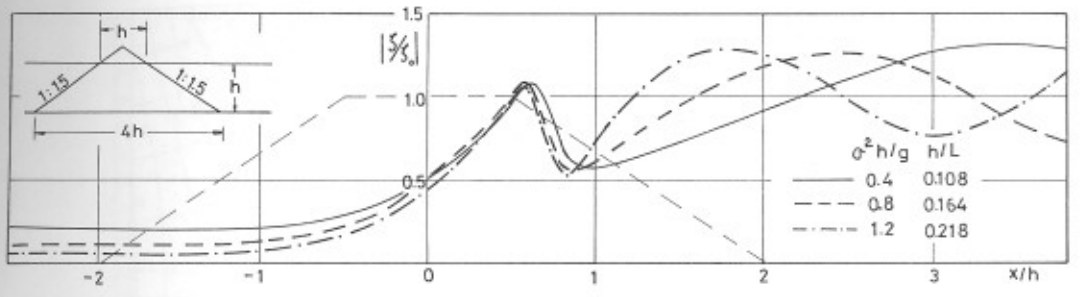


(a) ($V=0.5$, $\mu/\sigma=1.0$)

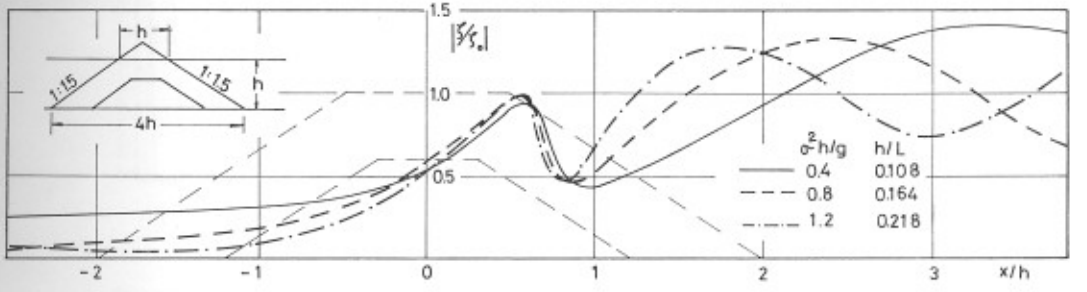


(b) ($V=0.5$, $\mu/\rho=1.0$)

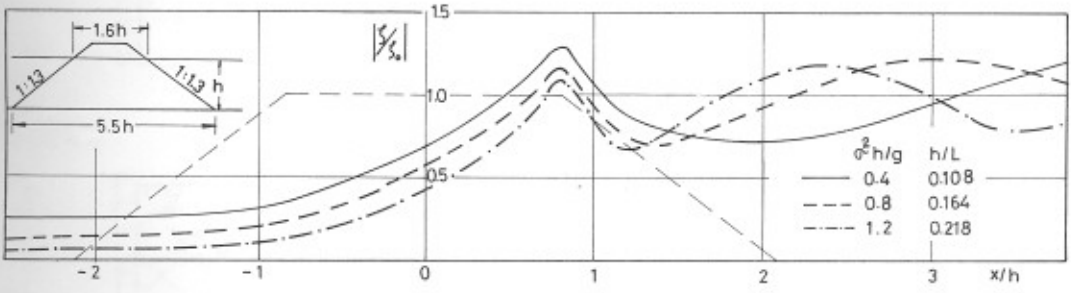


(c) ($V=0.5$, $\mu/\sigma=1.0$)

Fig. 8. Wave Height Distribution around Breakwater

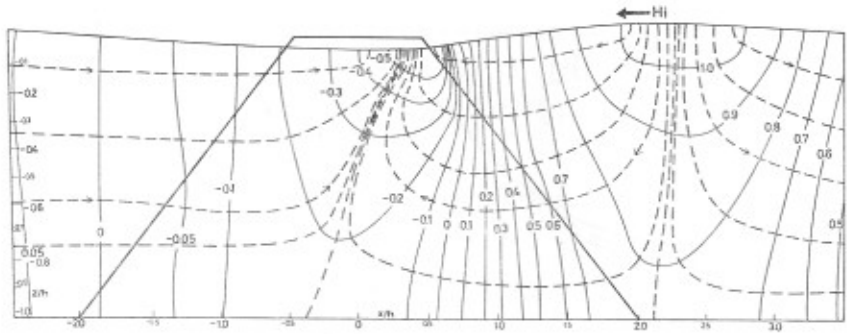


(a) $\sigma t = 0_{\circ}$

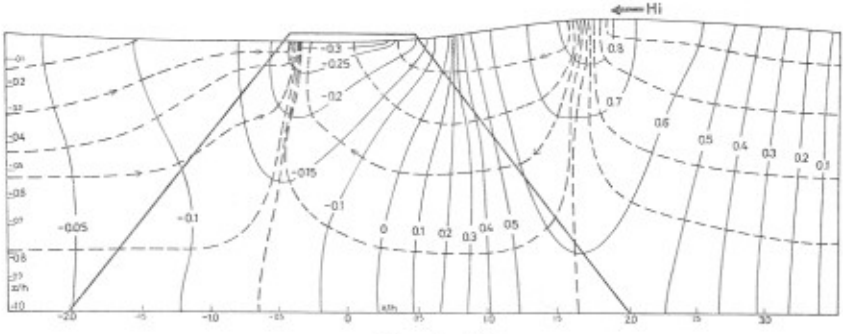


(b) $\sigma t = 30^{\circ}$

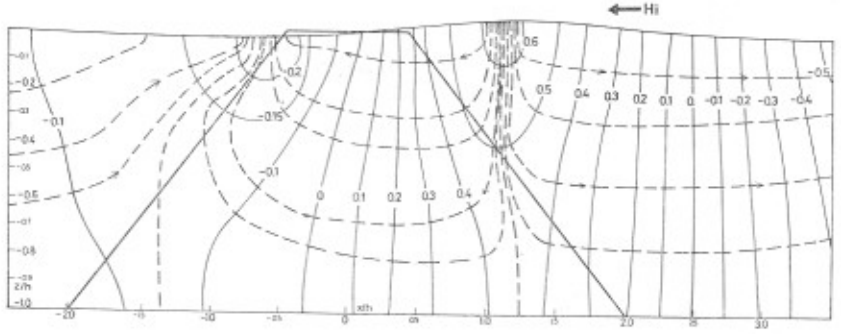


(c) $\sigma t = 60^{\circ}$

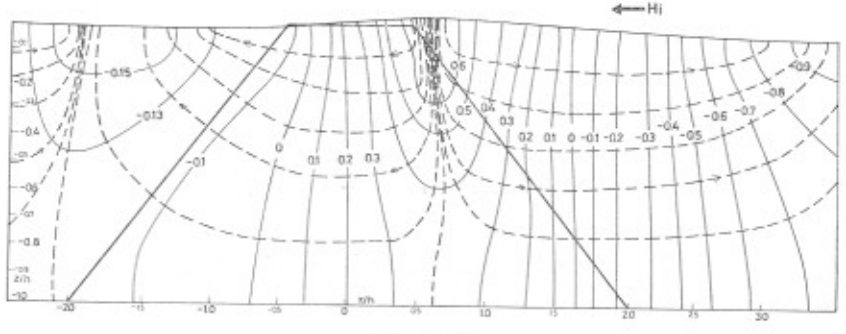


(d) $\sigma t = 90_{\circ}$

Fig. 9. Distribution of Velocity Potentials for Type A Breakwater, $\sigma^2 h/g = 0.6$

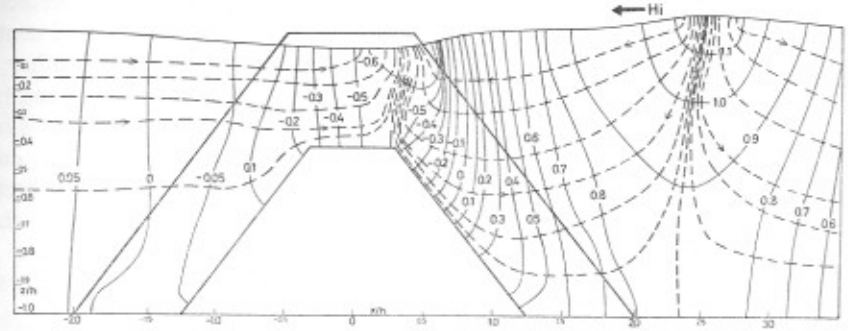


(a) $\sigma t = 0°$

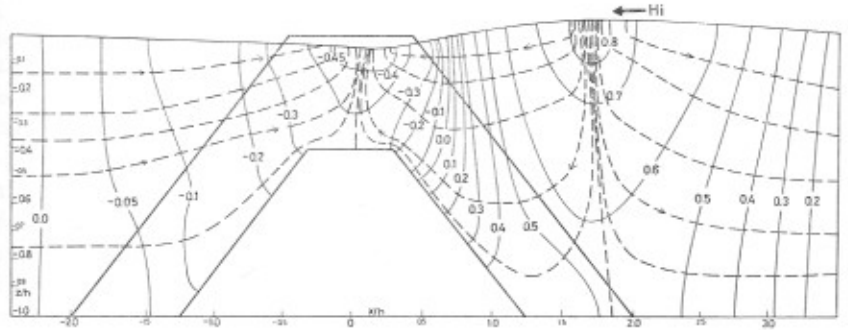


(b) $\sigma t = 30°$

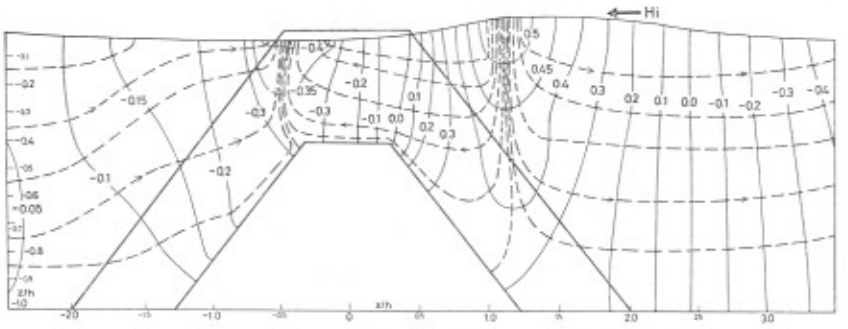


(c) $\sigma t = 60°$

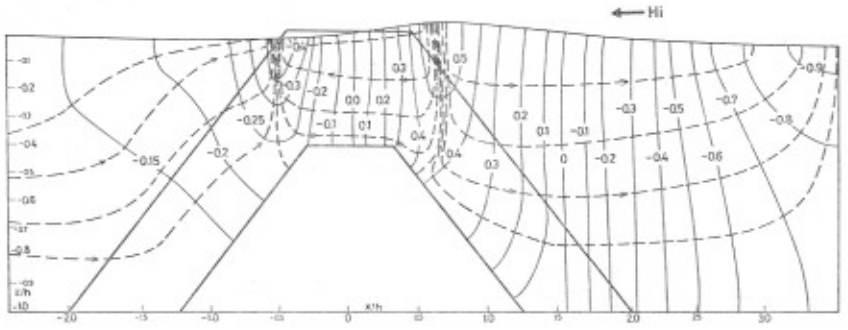


(d) $\sigma t = 90°$

Fig. 10. Distribution of Velocity Potentials for Type C Breakwater, $\sigma^2 h/g = 0.6$

(ii) Permeable breakwater with vertical faces

We consider the case when the breakwater of width $B=h$ and $2h$ are placed on the constant water depth $h$ or on the sloped bottom of foreside depth $h$ and rearside depth $0.5\,h$, as shown in Fig. 11, where the number of calculation points is shown in the figure. The calculated reflection-, transmission- and energy loss-coefficient for $V=0.5$ and $\mu/\sigma=1.0$ are shown in Fig. 12, where full lines are for constant water depth and broken lines are for sloped bottom. The calculated values

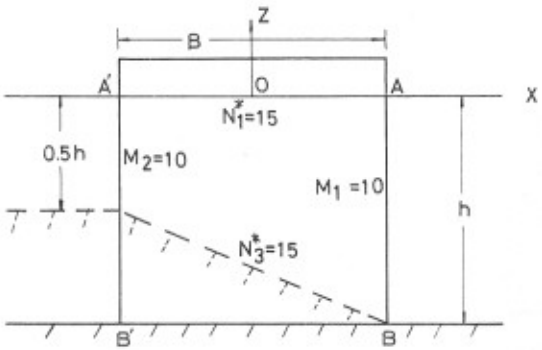


Fig. 11. Calculated Cross-Section of Vertical-Face Breakwater

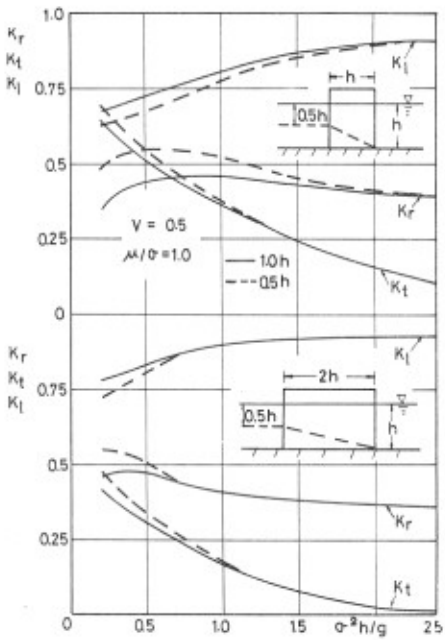


Fig. 12. $K_r$, $K_t$ and $K_l$ for Vertical-Face Breakwater

for the former one are in perfect agreement with those by the method of continuation of velocity potentials by the author (1971). It is clear that the reflection- and transmission coefficient for breakwater on sloped bottom are larger and energy loss coefficient is smaller than those for the breakwater on constant water depth, due to the reflection by sloped bottom, the increase of shoaling coefficient and the decrease in cross-sectional area in the former.

(iii) Permeable seawall with vertical- or sloped-face

Consider that permeable seawall whose width at still water level B is equal to the water depth $h$ or to $2h$ and whose slope of the face is 1 : 0 (vertical), 1 : 1 or 1 : 2 is placed in front of vertical impermeable wall and on the sea bed of depth $h$, as shown in Fig. 13. The calculated reflection- and energy loss-coefficient for $V=0.5$ and $\mu/\sigma=1.0$ are shown in Fig. 14, where full lines are vertical face, broken lines and dotted lines are for slope 1 : 1 and 1 : 2, respectively. The full lines for vertical face agree with the author's results (1971) by the method of continuation of velocity potentials.

In case of vertical face seawall, the reflection coefficients decrease remarkably as width B becomes wider for small $\sigma^2$ h/g but they asymtote independently on the width B to a certain value (0.35) for large $\sigma^2$ h/g. In seawall of 1 : 1 sloped-face, the reflection coefficients decrease in the similar manner to the above and they asymtote to another constant value (0.22) for large $\sigma^2$ h/g. While for seawall of 1 : 2 sloped-face, the reflection coefficients are larger than those for 1 : 1 slope as a whole, fluctuate rather irregularly with the change of $\sigma^2$ h/g and tend higher values than those for above two seawalls for large $\sigma^2$ h/g. And the effect of width B to the reflection coefficient is small for every $\sigma^2$ h/g. These facts suggest that when the slope of the face becomes too gentle, the fluid motion does not penetrate sufficiently into the porous material, so that the energy dissipation is depressed.

Fig. 15 shows the distribution of wave

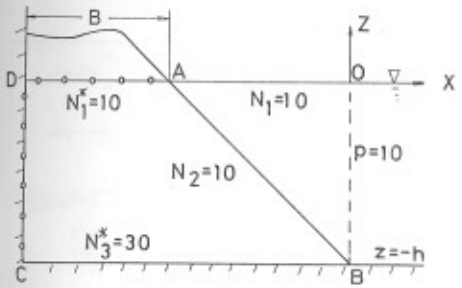


Fig. 13. Calculated Cross-Section of Permeable Sloped-Face Seawall

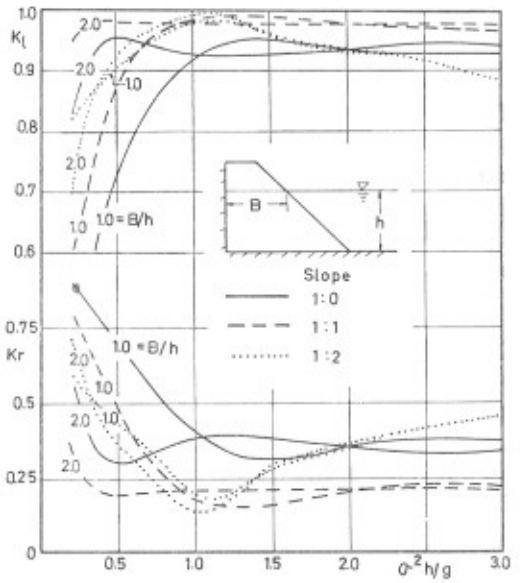


Fig. 14. $K_r$ and $K_t$ for Seawall with Vertical and Sloped Faces ($V=0.5$, $\mu/\sigma=1.0$)

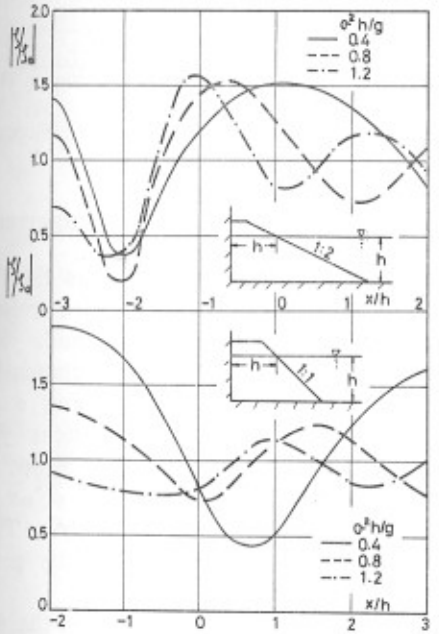


(a) ($V=0.5$, $\mu/\sigma=1.0$)

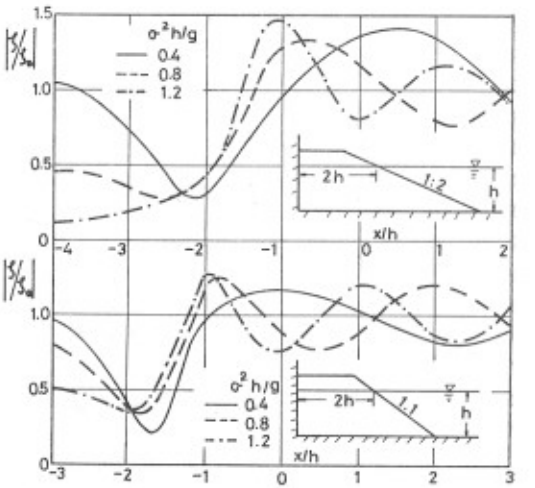


(b) ($V=0.5$, $\mu/\sigma=1.0$)

Fig. 15. Wave Height Distribution for Sloped-Face Seawall

height around seawall, from which it is found that the water surface fluctuation along the impermeable rear wall in 1 : 1 slope seawall is larger than that in 1 : 2 slope seawall, which means the fluid motion in the former is more active than that in the latter. (It should be noticed that the breaking effect of waves on sloped-face is ignored here.)

(iv) Underwater slope, beach profile and submerged breakwater

The calculated reflection and transmission coefficients for underwater slopes where the depth varies linearly from $h$ to $qh$ $(1>q>0)$ in the horizontal distance $h$ and $2h$ to the direction of wave progress are shown in Fig. 16 for $q=0.25$, 0.50 and 0.75. It is seen that the reflection coefficient becomes small for gentle slope, as expected. The calculated wave height distribution on beaches are shown in Fig. 17(a)(b)(c), where (a) is the distribution for beach profile formed by 1 : 1 slopes at both ends of flat shelf with depth $0.5h$ and length $2h$ continued from the constant water depth $h$, (b) is the one for the similar profile to above excepting the length of the flat shelf with length $3h$ and (c) is that for the profile with 1 : 2 slopes at both ends of the shelf with length $3h$. Every distribution has loops and nodes according to the values of $\sigma^2 h/g$ and wave height on flat shelf becomes somewhat larger than twice the incident wave height and the largest wave height of about 2.5 times the incident wave height appears for $\sigma^2 h/g \approx 0.8$ in Fig. (a), for $\sigma^2 h/g \approx 0.5$ in Fig. (b) and for $\sigma^2 h/g \approx 0.2$ in Fig. (c). These features are, of course, dependent not only on the length of shelf but also on the angle of slope.

Fig. 18 are the reflection coefficients for impermeable submerged breakwater whose cross-section is trapezoid of bottom width $B$, upper width $B'$ at the depth $qh$ $(1>q>0)$. Fig. (a) is the case for $B=h$, $B'=0.6h$, Fig. (b) is for $B=1.5h$, $B'=0.9h$, and Fig. (c) is for $B=2h$, $B'=1.2h$. In every case, $q$ is taken as 0.3, 0.4, 0.5 and 0.6. In these figures, it is notiable that non-reflection appears depending on the width and depth of upper face of the trapezoid. These features are similar to those of rectangular submerged breakwater calculated by the author (1971).**

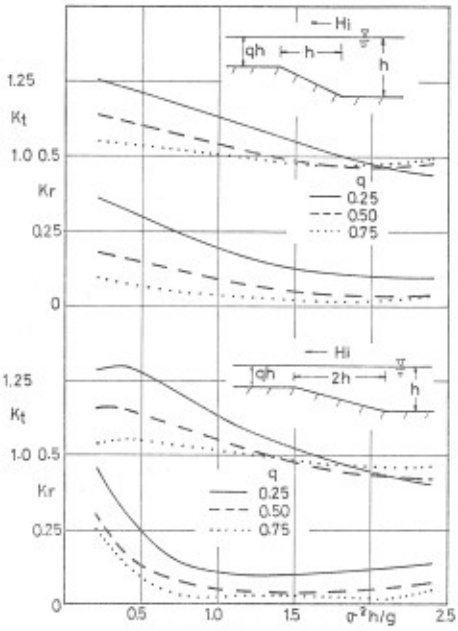


Fig. 16. $K_r$ and $K_t$ for Underwater Slopes

## XI Conclusions and Acknowledgement

It is made clear that as long as the fluid motion is of small amplitude with velocity potential, the Green's identity formula yields a system of geometrical linear relationships between boundary values of $\phi$ and $\bar{\phi}$ and the mechanical boundary conditions yield another system of linear relationships between them, from which $\phi$ and $\bar{\phi}$ on the boundary are determined uniquely. Then, Green's theorem provides the velocity potential wholly in the fluid region.

In above example of calculations, the fluid regions are bounded by straight lines, but this proposed method is preferably applied to the fluid region bounded by irregular curves. And also, even if the boundary is in oscillatory motion, this method is easily applied.

The authors express heartfelt thanks to the cooperation in computation work of Mr. Akinori Yoshida, the graduate student and

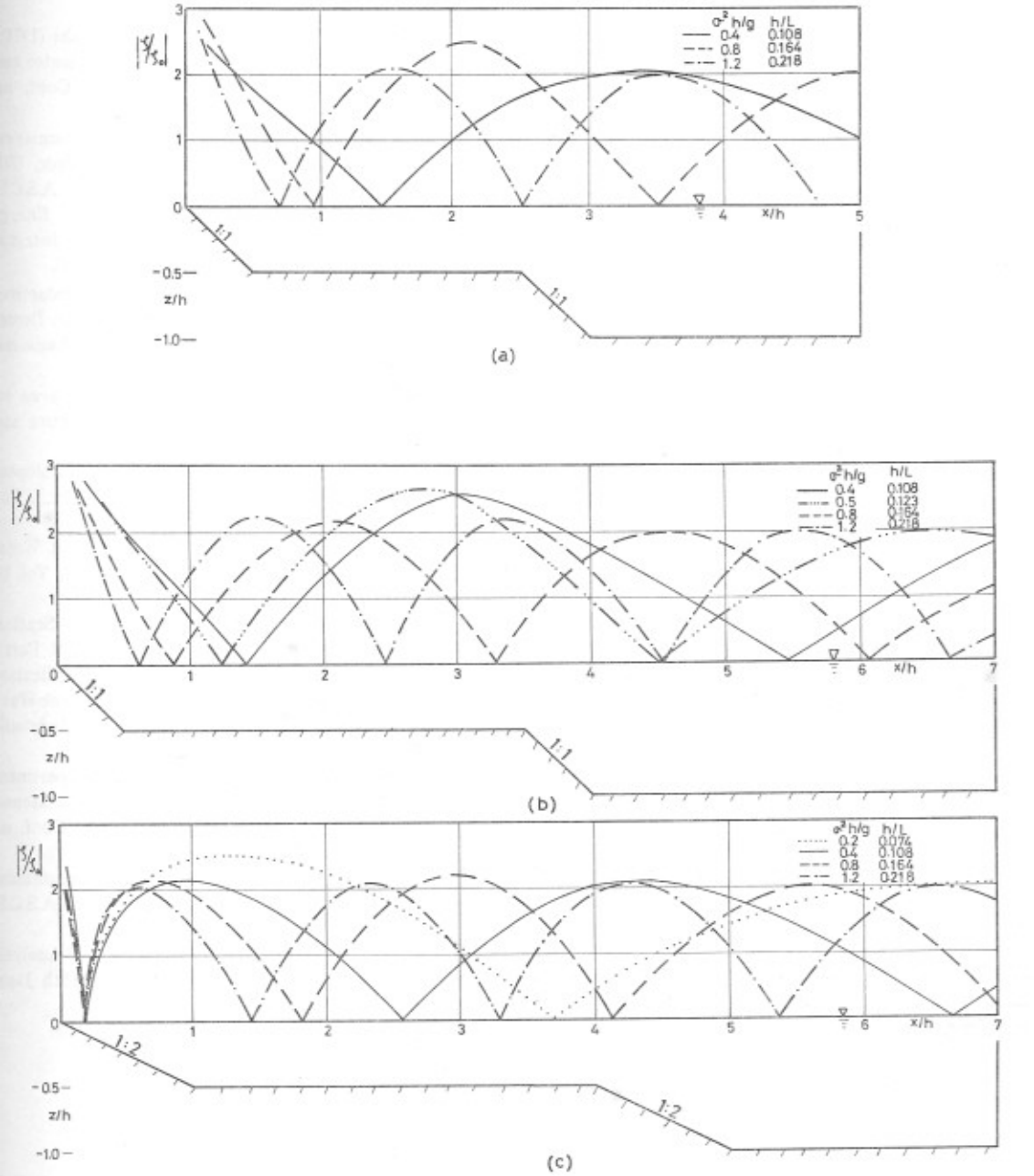


Fig. 17. Wave Height Distribution on Beach Step

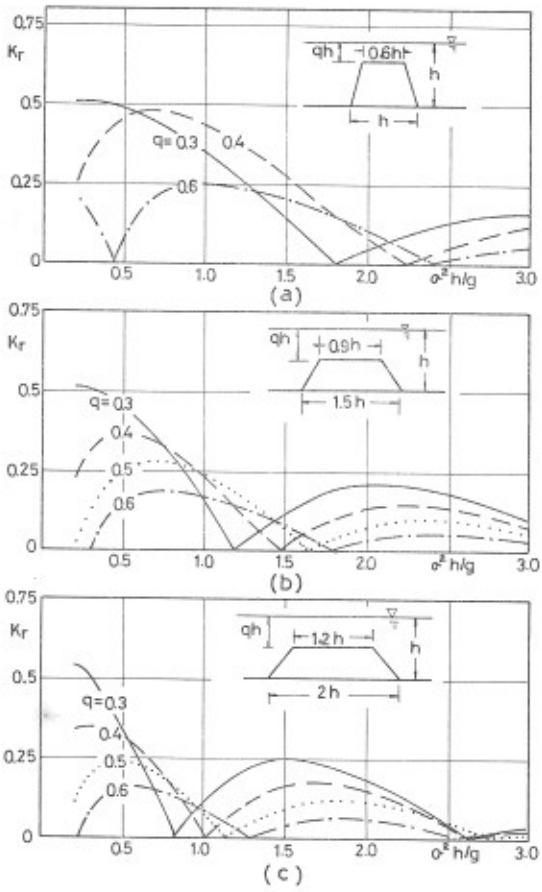


Fig. 18. $K_r$ of Impermeable Submerged Breakwater

Mrs. Yasu Yumura, the research assistant in the Department of Hydraulic Civil Engineering.

## Reference

(1) Ijima, T., Y. Eguchi and A. Kobayashi (1971): "Investigations on Permeable Breakwater and Quaywall." Proc. 18th Japanese Conf. on Coastal Eng. J.S.C.E. (In Japanese)

(2) Sollitt, C. K. (1972): "Wave Transmission through Permeable Breakwaters." Proc. 13th International Conf. on Coastal Eng. A.S.C.E.

(3) McCorquodale, J. A. (1972):" Wave Energy Dissipation in Rockfill." Proc. 13th International Conf. on Coastal Eng. A.S.C.E.

(4) Miche, M. (1944): "Mouvements Ondulatoires de la Mer en Profondeur Constante ou Decroisante." Annales des Ponts et Chaussées, Vol. 14, pp. 131~164

(5) Friedrichs, K. O. (1948): "Water Waves on a Shallow Sloping Beach." Comm. Pure and Applied Math. Vol.1, pp. 109~134

(6) Issacson, E. (1950):" Water Waves on Sloping Bottom." Com. Pure and Applied Math. Vol. 3, pp. 1~32

(7) Newman, J. N. (1965): "Propagation of Water Waves over an Infinite Step." J.F.M. Vol. 23, Part 2

(8) Miles, J. W. (1967): "Surface Wave Scattering Matrix for a Shelf." J.F.M. Vol. 28, Part 4

(9) Ijima, T. (1971*):" Analyses and Application of Boundary-Value Problems in Recent Wave Theories." Summer Seminor on Hydraulic Eng. J.S.C.E. (In Japanese)

(10) Hattori, M. and T. Sakai (1973):" Experiment on Wave Transmission through Rubble Mound Breakwater." Proc. 20th Japanese Conf. on Coastal Eng. J.S.C.E. (In Japanese)

(11) Madesen, O. S. (1974): "Wave Transmission through Porous Structures." Proc. A.S.C.E. Vol. 100, No. WW 3

(12) Ijima, T. and T. Sasaki (1971**): "Analysis on Submerged Breakwater." Proc. 18th Japanese Conf. on Coastal Eng. J.S.C.E. (In Japanese)